Simultaneous Wireless Power and Multi-Channel Data Transmission Based on OFDM

Yongzhi Jing, *Member, IEEE*, Xinjie Dan, Jialong Yu, Kang Fu, and Suleiman M. Sharkh, *Senior Member, IEEE*

***Abstract*—Aiming to meet the demand for multi-channel data communication between the power transmitter and receiver in a wireless power transfer system, a simultaneous wireless power and multi-channel data transmission method based on orthogonal frequency division multiplexing (OFDM) is proposed. In this method, a dual-*LC* resonant network is employed in the data transmitting circuits, which can achieve two independent data transmitting with only one data transmitting transformer. By making the power carrier and data carriers orthogonal to each other, the multi-channel data can be demodulated based on OFDM demodulation principle without requiring a filtering circuit and sampling resistance in the data receiving circuits. The power transmission adopts the bilateral *LCC* topological structure to achieve a load-independent constant current output. The data transmission characteristics are optimized by analyzing the system parameters impact on the data transmission gain. A 40 W experimental platform is built and a 4 × 85 kbps data transmission rate is achieved. Experimental results show that four-channel data in two forward and two backward channels can be transmitted accurately without interference from the power and other data carriers according to the OFDM principle. Moreover, the proposed system exhibits a high data bandwidth utilization.**

***Index Terms*—Bilateral *LCC*, multichannel data communication, orthogonal frequency division multiplexing (OFDM), wireless power transfer.**

I. Introduction

WIRELESS power transfer (WPT) technology can transmit electric power without the need for separable electrical contacts. Compared to traditional power transmission methods, it avoids issues such as electrical spark and leakage due to poor connection. Furthermore, it offers advantages, such as high flexibility, reliability, and low maintenance costs. Currently, WPT has been widely used in portable electronics, electric vehicles, industrial robots, and biomedical implants [1], [2], [3], [4].

The methods to achieve simultaneous wireless power and data transfer (SWPDT) mainly include separated and shared channel transmission technologies. Separated channel transmission technology achieves simultaneous power and data transmission by adding additional physical channels, mainly employing technologies, such as near field communication, Bluetooth, Wi-Fi, and ZigBee. However, these methods require complex pairing between the transmitter and receiver, causing significant communication delay [5], and making them unsuitable for certain specialized applications, such as real-time feedback control [6]. In addition, data transmission can also be achieved by using additional coupling coils, but the interference between the power and data transmission coils must be taken into account in this approach, which increases the complexity of system. Shared channel transmission technology adopts the same physical channel to achieve simultaneous power and data transmission, which is widely used in SWPDT system because of the simplicity and high reliability [7], [8], [9], [10].

The data loading method in the shared SWPDT system mainly includes power modulation and independent carrier injection. Power modulation employs the power carrier as a medium to modulate the data by altering the amplitude, phase, or frequency of the power carrier [11], [12], [13], [14], but the stability of power transmission may be impacted. In [11], information, such as efficiency, voltage and current, can be transferred to the main server by using the equivalent parallel resonant capacitance for impedance modulation operation, but the data transmission rate is relatively low. Independent carrier injection method uses an independent carrier with higher frequency than the power carrier for data modulation, so that high data transmission rate can be realized, and the data transmission circuits are typically connected in parallel or in series with the power circuits to inject and extract the data.

However, the interference between power and data inevitably occurs in the shared transfer channel, and achieving accurate data separation and demodulation is difficult using simple analog filtering circuits, especially in multi-channel data transmission systems. In [15] and [16], a four resonance dual-rejection structure and dual-notch filter are used in the SWPDT system to suppress the crosstalk between the forward and backward data of full-duplex communication, respectively, but these methods need many passive components,

Manuscript received 5 December 2023; revised 17 February 2024; accepted 9 March 2024. Date of publication 14 March 2024; date of current version 16 May 2024. This work was supported in part by the National Natural Science Foundation of China under Grant 52077183 and Grant 52372364, and in part by the China Scholarship Council. Recommended for publication by Associate Editor X. Ruan. *(Corresponding author: Yongzhi Jing.)*

Yongzhi Jing is with the Key Laboratory of Magnetic Suspension Technology and Maglev Vehicle, Ministry of Education, Chengdu 610031, China, also with the School of Electrical Engineering, Southwest Jiaotong University, Chengdu 610031, China, and also with the Department of Mechanical Engineering, University of Southampton, SO17 1BJ Southampton, U.K. (e-mail: jingyongzhi@swjtu.edu.cn).

Xinjie Dan and Jialong Yu are with the School of Electrical Engineering, Southwest Jiaotong University, Chengdu 610031, China (e-mail: danxinjie@my.swjtu.edu.cn; qq1017861072@my.swjtu.edu.cn).

Kang Fu is with the Tangshan Graduate School of Southwest Jiaotong University, Tangshan 063000, China (e-mail: fukang@my.swjtu.edu.cn).

Suleiman M. Sharkh is with the Department of Mechanical Engineering, University of Southampton, SO17 1BJ Southampton, U.K. (e-mail: suleiman@soton.ac.uk).

Color versions of one or more figures in this article are available at https://doi.org/10.1109/TPEL.2024.3377260.

Digital Object Identifier 10.1109/TPEL.2024.3377260

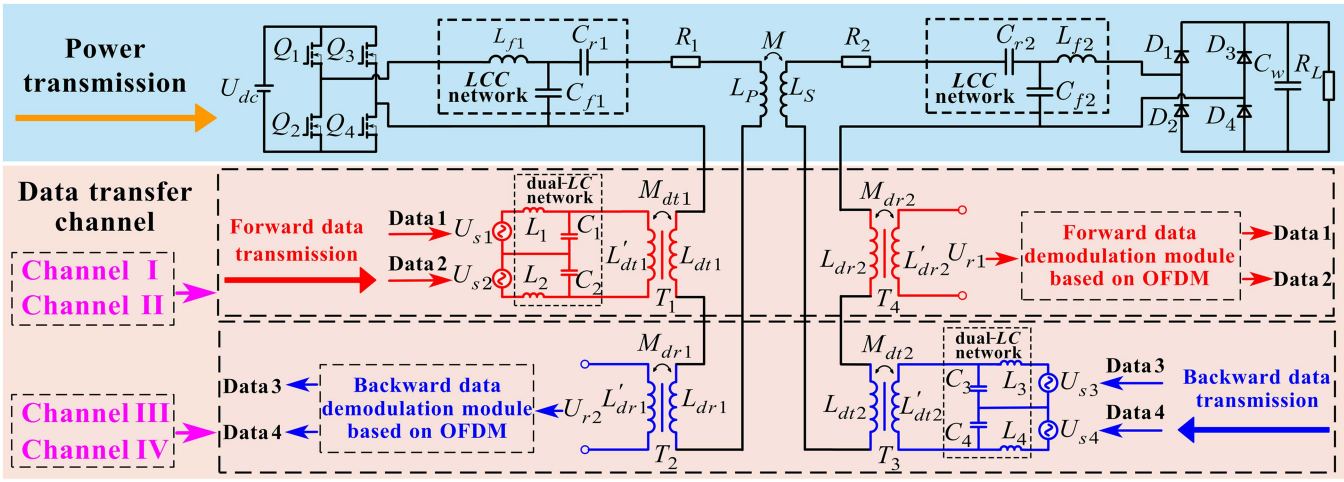

Fig. 1. Simultaneous power and multi-channel data transmission system based on OFDM.

which increases the system's complexity. In [17], the differential quadrature phase shift keying (DQPSK) is used to achieve full-duplex communication with a simple system structure, but the utilization of bandwidth is relatively low. Moreover, in these articles, their full-duplex communications are all based on single forward and backward data, which is difficult to apply to multi-channel data transmission. In some particular systems, e.g., EV chargers, chargers for air or underwater drones where additional data communications need be exchanged between the transmitter and receiver, such as user IDs, battery management information and power billing data, collected drone video, which are usually separate from the system control data transmission. For high-speed and stable communication through multi-channel data, a hybrid modulation waves PWM control method is used in [18] to realize multi-bit signals transmission through several channels. However, simultaneous forward and backward bidirectional transmission of multibit signals cannot be realized, and the high switching frequency will cause more power electronic converter switching losses.

Aiming to address the aforementioned issues, this article proposes a simultaneous wireless power and multi-channel data transmission method based on OFDM. The key contributions of this article are as follows.

1) A dual-*LC* resonant network is proposed and designed in the data transmitting circuits, which can achieve two independent data transmitting using just one data transmitting transformer, giving a novel method for multi-channel data transmission with a simpler circuit and fewer data transmitting transformers.
2) A full-duplex communication with four data channels is achieved based on the OFDM principle by ensuring the power and all data carriers are orthogonal, which theoretically eliminates interference of power on data transmission, as well as crosstalk between data carriers, and achieves higher utilization of bandwidth.
3) The proposed system does not require any filtering network and sampling resistor in the data receiving circuits, which greatly simplifies the system structure.

The rest of this article is organized as follows. Section II gives an overview of the proposed system, mainly including the structure configuration of the power and data transmission. Section III analyzes the transfer characteristics of power and data, and presents the design method used to select the system parameters. Section IV introduces the OFDM demodulation principle. Section V presents experimental results to validate the theoretical analysis. Finally, Section VI concludes this article.

II. Overview of the Proposed System

The structure of the simultaneous wireless power and multi-channel data transmission system based on OFDM is shown in Fig. 1. The power transmission circuit consists of a dc power supply, a full-bridge inverter, loosely coupled coils, bilateral *LCC* networks, a full-bridge rectifier circuit, and the load R_L. The data transfer channel consists of modulated data sources, dual-*LC* networks, data coupling transformers, data demodulation modules. The injection and extraction of each data are achieved by connecting the data transformers in series with the power transmission circuit. A dual-*LC* resonance network is employed in the data transmitting circuit to send two channel data simultaneously by sharing one data transmitting transformer. In the data receiving circuit, only one shared data receiving transformer is used to extract the data transmitted by both channels on the opposite side. The data demodulation module directly acquires the voltage on the secondary side of the data receiving transformer, and the data from each channel can be restored based on OFDM without interference with each other.

In the power transmission circuit, the bilateral *LCC* topology structure is used to achieve the load-independent constant current output. Capacitors C_{f1} and C_{f2} provide additional return paths for the higher harmonics, so this topology is also used to filter out a large portion of the high-order harmonics generated by the inverter and rectifier. Q_1–Q_4 are the four MOSFETs of the full-bridge inverter circuit. D_1–D_4 are the four diodes of the full-bridge rectifier circuit. L_P and L_S are the self-inductances of the primary and secondary coils of the loosely coupled

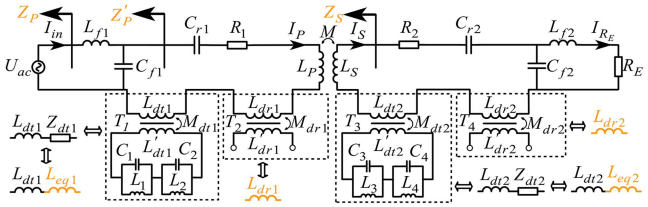

Fig. 2. Power transmission equivalent circuit.

transformer, respectively. L_{dt1} and L'_{dt1}, L_{dr1} and L'_{dr1}, L_{dt2} and L'_{dt2}, L_{dr2} and L'_{dr2}, are the self-inductances of the primary and secondary coils of the data transmission transformers T_1–T_4. L_{f1}, C_{f1}, and C_{r1} consist of the primary side resonance compensation network, and the L_{f2}, C_{f2}, and C_{r2} consist of the secondary side resonance compensation network.

According to the bilateral *LCC* compensation principle [19], the parameters of resonant network in the power transmission circuit should satisfy

$$\begin{cases} \omega_p = 1/\sqrt{L_{f1}C_{f1}} \\ \quad = 1/\sqrt{(L_P + L_{dt1} + L_{dr1} + L_{eq1} - L_{f1})C_{r1}} \\ \omega_p = 1/\sqrt{L_{f2}C_{f2}} \\ \quad = 1/\sqrt{(L_S + L_{dt2} + L_{dr2} + L_{eq2} - L_{f2})C_{r2}} \end{cases} \tag{1}$$

where $\omega_p = 2\pi f_p$ is the angular frequency of the power carrier, f_p is the frequency of the power carrier, L_{eq1} and L_{eq2} are the equivalent inductances reflected from the forward and backward data transmitting circuits to the power transmission circuit in the under-resonance state, respectively.

In the data transmitting circuits, L_1, C_1, L_2, and C_2 consist of the forward data transmitting dual-*LC* network, and the L_3, C_3, L_4 and C_4 consist of the backward data transmitting dual-*LC* network. Setting the *n*th data carrier frequency of the four data is f_{sn}, and the *LC* resonant network parameters of each data should satisfy

$$\omega_{sn} = 1/\sqrt{L_n C_n} \tag{2}$$

where $\omega_{sn} = 2\pi f_{sn}$ (n = 1, 2, 3, 4) is the angular frequency of the *n*th data carrier.

III. Analysis of Transfer Characteristic

A. Power Transfer Characteristic

When analyzing the power transfer characteristics without data transmission, the four data sources U_{s1}–U_{s4} are treated as short circuits, and the power transmission equivalent circuit is shown in Fig. 2.

Due to the good frequency selection characteristic of the bilateral *LCC* compensation structure, the dc source and full-bridge inverter are equivalent to an ideal ac source U_{ac} based on fundamental harmonic approximation, the full-bridge rectifier circuit and load R_L are equivalent to an ac load resistance R_E, and the conversion formula is given by

$$\begin{cases} U_{ac} = 2\sqrt{2}U_{dc}/\pi \\ R_E = 8R_L/\pi^2 \end{cases}. \tag{3}$$

There are the reflected impedances from the data transmitting and receiving circuits to the power side; the reflected impedance of the forward and backward data transmitting circuits are designated as Z_{dt1} and Z_{dt2}; the reflected impedance of the backward and forward data receiving circuits are designated as Z_{dr1} and Z_{dr2}; and the reflected impedances can be calculated as

$$\begin{cases} Z_{dt1} = (\omega_p M_{dt1})^2/Z'_{dt1} \\ Z_{dt2} = (\omega_p M_{dt2})^2/Z'_{dt2} \end{cases} \quad \begin{cases} Z_{dr1} = (\omega_p M_{dr1})^2/Z'_{dr1} \\ Z_{dr2} = (\omega_p M_{dr2})^2/Z'_{dr2} \end{cases} \tag{4}$$

where M_{dt1}, M_{dr1}, M_{dt2}, M_{dr2} are the mutual inductances of transformers T_1-T_4, respectively, and Z'_{dt1}, Z'_{dr1}, Z'_{dt2}, Z'_{dr2} are the self-impedances of the data transmitting and receiving circuits. Form Fig. 2, it can be seen that the impedances Z'_{dr1} and Z'_{dr2} are at high-impedance, so Z_{dr1} and Z_{dr2} can be neglected because they are at low-impedance and are close to zero according to the (4). The self-impedances of the data transmitting circuits can be calculated as

$$\begin{cases} Z'_{dt1} = j\omega_p L_1 // (1/j\omega_p C_1) \\ \qquad + j\omega_p L_2 // (1/j\omega_p C_2) + j\omega_p L'_{dt1} \\ Z'_{dt2} = j\omega_p L_3 // (1/j\omega_p C_3) \\ \qquad + j\omega_p L_4 // (1/j\omega_p C_4) + j\omega_p L'_{dt2} \end{cases}. \tag{5}$$

From (5), it can be seen that the Z'_{dt1} and Z'_{dt2} are not in high-impedance state at the power frequency, their reflected impedances Z_{dt1} and Z_{dt2} cannot be neglected, which need to be considered in the bilateral *LCC* compensation calculation. Since the data carrier frequencies are all higher than the power frequency, the dual-*LC* resonance networks in the data transmitting circuits are in the under-resonance state at the power frequency, and exhibit purely inductive characteristics when the resistances in the data transmitting circuits are negligible, therefore the reflected impedances Z_{dt1} and Z_{dt2} can also be represented as

$$\begin{cases} Z_{dt1} = j\omega_p L_{eq1} \\ Z_{dt2} = j\omega_p L_{eq2} \end{cases}. \tag{6}$$

The power transmitting and receiving circuit impedances Z_P and Z_S can be calculated as

$$\begin{cases} Z_P = j\omega_p L_{f1} + (1/j\omega_p C_{f1}) // Z'_P \\ Z'_P = 1/j\omega_p C_{r1} + j\omega_p (L_P + L_{dt1} + L_{dr1} + L_{eq1}) \\ \qquad + R_1 + Z_{SP} \\ Z_S = (R_E + j\omega_p L_{f2}) // (1/j\omega_p C_{f2}) + 1/j\omega_p C_{r2} \\ \qquad + j\omega_p (L_S + L_{dt2} + L_{dr2} + L_{eq2}) + R_2 \end{cases} \tag{7}$$

where $Z_{SP} = (\omega_p M)^2/Z_S$ is the impedance reflected from the secondary side to the primary side in the power transmission circuit, R_1 and R_2 are the internal resistances of the loosely coupled coils.

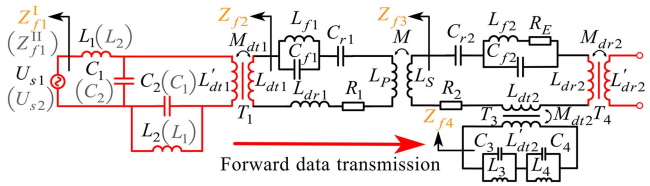

Fig. 3. Equivalent circuit of the forward data transfer channels I and II.

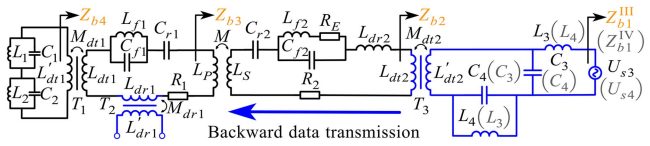

Fig. 4. Equivalent circuit of the backward data transfer channels III and IV.

According to the KCL, the currents I_P and I_S in the primary and secondary sides of the loosely coupled coils can be obtained by

$$\begin{cases} I_P = I_{in}\frac{1/j\omega_p C_{f1}}{1/j\omega_p C_{f1}+Z'_P} \\ I_S = j\omega_p M I_P / Z_S \end{cases}. \tag{8}$$

The current I_{R_E} in the equivalent ac load resistance R_{E} can be calculated by

$$I_{R_E} = I_S \frac{1/j\omega_p C_{f2}}{1/j\omega_p C_{f2} + j\omega_p L_{f2} + R_E} \tag{9}$$

and if the internal resistances of the loosely coupled coils R_1 and R_2 are neglected, the I_{R_E} can be simplified as

$$I_{R_E} = \frac{MU_{ac}}{\omega_p L_{f1} L_{f2}}. \tag{10}$$

According to the (10), the output load current I_{R_E} is proportional to M and U_{ac}, inversely proportional to ω_p, L_{f1}, L_{f2}, and independent of the load resistance R_E, so the system has a load-independent constant current output characteristic.

Combining (1), (7), (8), and (9), the system efficiency η can be obtained as

$$\eta = \frac{P_{\mathrm{out}}}{P_{\mathrm{in}}} = \frac{I_{R_E}^2 R_E}{U_{ac} I_{in}} = \frac{M^2 R_E}{(R_1 + Z_{SP})[C_{f2}(R_2 R_E + \omega_p^2 L_{f2}^2)]^2}. \tag{11}$$

It can be seen that the efficiency η is mainly related to the mutual inductance M of the loosely coupled coils, the power frequency ω_p, the load resistor R_E, and the loosely coupled coils internal resistances R_1 and R_2, so the efficiency of the system can be improved by increasing the mutual inductance M and decreasing the internal resistances R_1 and R_2.

B. Data Transfer Characteristic

When analyzing the transfer characteristic of one forward data channel, the power supply and other data sources are treated as short circuits, and the equivalent circuit of forward data transfer channel I and II is shown in Fig. 3. Data channels I and II have the same circuit structure differing only in data transmitting circuit parameters, so the equivalent circuit of data channel II can be obtained by exchanging the positions of L_1 and C_1 with L_2 and C_2, respectively.

The forward modulated signal is injected into the forward data transmitting transformer T_1 and extracted from the secondary side of forward data receiving transformer T_4. Since the impedance of data transmission in the power transfer circuit is significantly larger than the resistance of the loosely coupled coils, the influence of R_1 and R_2 on the data transmission can be neglected, and the impedances of each part in the forward data transfer channel I and II can be obtained as

$$\begin{cases} Z_{f1}^{\mathrm{I}} = sL_1 + (1/sC_1)//\left[-(sM_{dt1})^2/Z_{f2} \right. \\ \qquad \left. + sL'_{dt1} + sL_2 // (1/sC_2)\right] \\ Z_{f1}^{\mathrm{II}} = sL_2 + (1/sC_2)//\left[-(sM_{dt1})^2/Z_{f2} \right. \\ \qquad \left. + sL'_{dt1} + sL_1 // (1/sC_1)\right] \\ Z_{f2} = -(sM)^2/Z_{f3} + sL_P + sL_{dt1} + sL_{dr1} \\ \qquad + sL_{f1} // (1/sC_{f1}) + 1/sC_{r1} \\ Z_{f3} = -(sM_{dt2})^2/Z_{f4} + sL_S + sL_{dt2} + sL_{dr2} \\ \qquad + 1/sC_{r2} + (sL_{f2} + R_E) // (1/sC_{f2}) \\ Z_{f4} = sL_3//(1/sC_3) + sL_4//(1/sC_4) + sL'_{dt2} \end{cases} \tag{12}$$

where $Z^{\mathrm{I}}{}_{f1}$ and $Z^{\mathrm{II}}{}_{f1}$ are the self-impedances of data transmitting circuit when forward data 1 and data 2 are transmitted individually, and data channels I and II have the same Z_{f2}, Z_{f3}, and Z_{f4}. The transfer functions of each part in the forward data transfer channel can be obtained as

$$\begin{cases} G_{f1}^{\mathrm{I}} = (1/Z_{f1}^{\mathrm{I}})\,(1/sC_1)\,/\left[-(sM_{dt1})^2/Z_{f2} \right. \\ \qquad \left. + (1/sC_1) + sL'_{dt1} + sL_2 // (1/sC_2)\right] \\ G_{f1}^{\mathrm{II}} = (1/Z_{f1}^{\mathrm{II}})(1/sC_2)/\left[-(sM_{dt1})^2/Z_{f2} \right. \\ \qquad \left. + (1/sC_2) + sL'_{dt1} + sL_1 // (1/sC_1)\right] \end{cases}$$

$$\begin{cases} G_{f2} = sM_{dt1} \\ G_{f3} = 1/Z_{f2} \\ G_{f4} = sM \\ G_{f5} = 1/Z_{f3} \\ G_{f6} = sM_{dr2} \end{cases}. \tag{13}$$

According to (13), the transmission gains of data channels I and II can be obtained as

$$\begin{cases} G_{s1} = U_{r1}/U_{s1} = G_{f1}^{\mathrm{I}} G_{f2} G_{f3} G_{f4} G_{f5} G_{f6} \\ G_{s2} = U_{r1}/U_{s2} = G_{f1}^{\mathrm{II}} G_{f2} G_{f3} G_{f4} G_{f5} G_{f6} \end{cases} \tag{14}$$

where U_{r1} is the voltage on the secondary side of the forward data receiving transformer T_4, U_{s1} and U_{s2} are the source voltages of data 1 and 2, respectively.

The process of backward data transmission is similar to the forward data transmission. The backward data transfer equivalent circuit of channels III and IV is shown in Fig. 4. The equivalent circuit of data channel IV can be obtained by exchanging the positions of L_3 and C_3 with L_4 and C_4, respectively.

The impedance of each part of backward data transmission can be obtained as

$$\begin{cases} Z_{b1}^{\mathrm{III}} = sL_3 + \left(1/sC_3\right) //\left[-(sM_{dt2})^2/Z_{b2} \right. \\ \qquad \left. +sL'_{dt2} + sL_4 // \left(1/sC_4\right)\right] \\ Z_{b1}^{\mathrm{IV}} = sL_4 + \left(1/sC_4\right) //\left[-(sM_{dt2})^2/Z_{b2} \right. \\ \qquad \left. +sL'_{dt2} + sL_3 // \left(1/sC_3\right)\right] \\ Z_{b2} = -(sM)^2/Z_{b3} + sL_S + sL_{dt2} + sL_{dr2} + 1/sC_{r2} \\ \qquad + \left(sL_{f2} + R_E\right) // \left(1/\mathrm{s}C_{f2}\right) \\ Z_{b3} = -(sM_{dt1})^2/Z_{b4} + sL_P + sL_{dt1} + sL_{dr1} \\ \qquad +1/sC_{r1} + sL_{f1} // \left(1/sC_{f1}\right) \\ Z_{b4} = sL_1 // \left(1/sC_1\right) + sL_2 // \left(1/sC_2\right) + sL'_{dt1} \end{cases} \tag{15}$$

where $Z^{\mathrm{III}}{}_{b1}$ and $Z^{\mathrm{IV}}{}_{b1}$ are the self-impedances of data transmitting circuit when backward data 3 and data 4 are transmitted individually, then the transfer functions of each part in the backward data transfer channel can be obtained as

$$\begin{cases} G_{b1}^{\mathrm{III}} = (1/Z_{b1}^{\mathrm{III}})(1/sC_3)/\left[-(sM_{dt2})^2/Z_{b2} \right. \\ \qquad \left. +(1/sC_3) + sL'_{dt2} + sL_4 // \left(1/sC_4\right)\right] \\ G_{b1}^{\mathrm{IV}} = (1/Z_{b1}^{\mathrm{IV}})(1/sC_4)/\left[-(sM_{dt2})^2/Z_{b2} \right. \\ \qquad \left. + \left(1/sC_4\right) + sL'_{dt2} + sL_3 // \left(1/sC_3\right)\right] \end{cases}$$

$$\begin{cases} G_{b2} = sM_{dt2} \\ G_{b3} = 1/Z_{b2} \\ G_{b4} = sM \\ G_{b5} = 1/Z_{b3} \\ G_{b6} = sM_{dr1} \end{cases} . \tag{16}$$

According to (16), the transmission gains of data channels III and IV can be obtained as

$$\begin{cases} G_{s3} = U_{r2}/U_{s3} = G_{b1}^{\mathrm{III}} G_{b2} G_{b3} G_{b4} G_{b5} G_{b6} \\ G_{s4} = U_{r2}/U_{s4} = G_{b1}^{\mathrm{IV}} G_{b2} G_{b3} G_{b4} G_{b5} G_{b6} \end{cases} \tag{17}$$

where U_{r2} is the voltage on the secondary side of the backward data receiving transformer T_2, U_{s3} and U_{s4} are the source voltages of data 3 and data 4, respectively.

It can be seen that the forward and backward data transmission characteristics are similar and are both related to the data carrier frequency, the self-inductances of the data transmission transformers T_1-T_4, the self-inductances and mutual inductance of the loosely coupled coils, the resistances R_1 and R_2, as well as the dual-*LC* resonant network in data transmitting circuits. The self-inductance, mutual inductance, and internal resistances of the loosely coupled coils are determined by the power transmission requirement, so it is only necessary to consider the effect of the data carrier frequency, the self-inductance of the data transmission transformers, and the dual-*LC* resonant networks on data transmission.

To simplify the analysis and maintain the symmetry of data transfer circuits in the parameters design, it is assumed that the

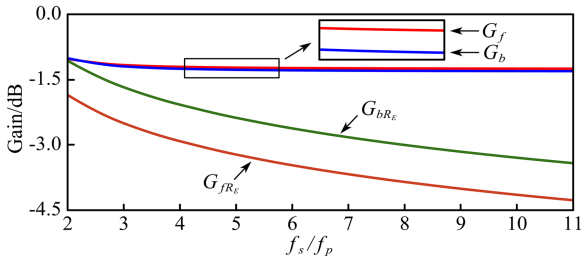

Fig. 5. Transmission gains G_f, G_b, G_{fR_E}, and G_{bR_E} versus data carrier frequency.

parameters of the data transmission transformers and the dual-*LC* resonant networks satisfy

$$\begin{cases} L_{dt1} = L'_{dt1} = L_{dt2} = L'_{\mathrm{dt2}} = L_{dt} \\ L_{dt1} = L'_{dr1} = L_{dr2} = L'_{dr2} = L_{dr} \\ L_1 = L_2 = L_3 = L_4 = L_d \end{cases} \quad \begin{cases} M_{dt1} = M_{dt2} \\ M_{dr1} = M_{dr2} \end{cases} . \tag{18}$$

In order to select the appropriate frequencies for the four data carriers, it is necessary to analyze the relationship between data transmission characteristics and data carrier frequency. By connecting the data sources directly to the data transmitting transformers, the forward and backward data transmission gains G_f and G_b, and the forward and backward data to load gains G_{fR_E} and G_{bR_E} can be obtained as

$$\begin{cases} G_f = \left(1/sL'_{\mathrm{dt1}}\right) G_{f2} G_{f3} G_{f4} G_{f5} G_{f6} \\ G_b = \left(1/sL'_{dt2}\right) G_{b2} G_{b3} G_{b4} G_{b5} G_{b6} \\ G_{fR_E} = \left(1/sL'_{\mathrm{dt1}}\right) G_{f2} G_{f3} G_{f4} G_{f5} G_{R_E} \\ G_{bR_E} = \left(1/sL'_{dt2}\right) G_{b2} G_{b3} G_{R_E} \end{cases} \tag{19}$$

where G_{R_E} is the transfer function from the secondary side of the power to the load R_E, which can be calculated as

$$G_{R_E} = R_E \left(1/sC_{f2}\right)/(sL_{f2} + R_E + 1/sC_{f2}). \tag{20}$$

The relationship between the transmission gain and the data carrier frequency is shown in Fig. 5. It can be seen that the G_f, G_b, G_{fR_E}, and G_{bR_E} all decrease with the increase of data carrier frequency, the G_{fR_E} and G_{bR_E} are much lower than the G_f and G_b, and the G_f is slightly higher than the G_b. It is worth noting that the G_{bR_E} is overall higher than the G_{fR_E}, this is because that the transmission path of forward data to the load is longer than that of the backward data, which suppresses the forward data transmission more than the backward transmission, and hence the backward data requires a higher carrier frequency than the forward data to minimize the impact on the load.

In order to ensure the orthogonality among the power carrier and data carriers, each data frequency should be set as an integer multiple of the power carrier frequency. Considering the transmission gain of the data itself and the effect of data transmission on the load R_E, the four data carrier frequencies can be selected as $f_{s1} = 3f_p, f_{s2} = 5f_p, f_{s3} = 7f_p, f_{s4} = 9f_p$, where f_p is the power carrier frequency with a value of 85 kHz. The four data carrier frequencies are separated by only one power

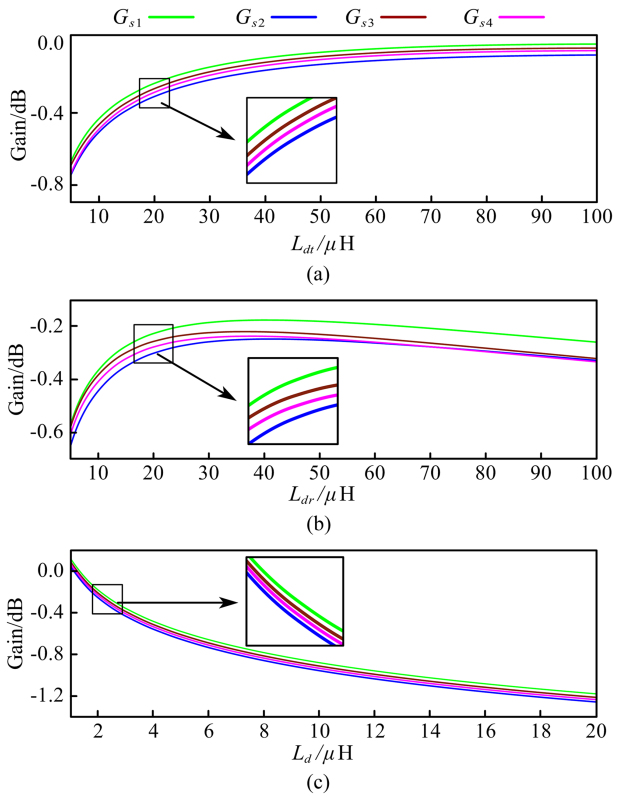

Fig. 6. Data transfer channel gains G_{s1}–G_{s4} versus (a) L_{dt}, (b) L_{dr} and (c) L_d.

frequency f_p so that the data frequency bandwidth can be fully utilized.

After determining the data carrier frequencies, the relationship between the four data transfer channel gains G_{s1}–G_{s4} and the system parameters L_{dt}, L_{dr}, and L_d can be obtained as shown in Fig. 6, and it can be seen that the four data transfer channel gains have approximate characteristic curves due to similar circuit structures. From the Fig. 6(a), the transmission gains of the four data channels all increase with the increase of L_{dt}, but the increasing trend is not obvious when L_{dt} exceeds 20 μH, so the L_{dt} is selected as 20 μH in consideration of the transformer size, power consumption and voltage tolerance. From the Fig. 6(b), as the increase of L_{dr}, the transmission gains of the four data channels show a tendency of increasing and then decreasing, and the maximum gain occurs in the range of 20–30 μH, so the L_{dr} is selected as 20 μH. From the Fig. 6(c), the four data transfer channels gains decrease with the increase of L_d, so L_d can be reduced to improve the data transfer channel gains, but too small L_d will increase the value of the resonant capacitance matched with it, which will increase the size of system, so the value of L_d is selected as 2.2 μH for comprehensive consideration.

IV. OFDM Demodulation Principle

In the time domain, if two sinusoids satisfy

$$\int_a^b \sin(\omega_1 t)\cdot\sin(\omega_2 t)\,dt = 0 \tag{21}$$

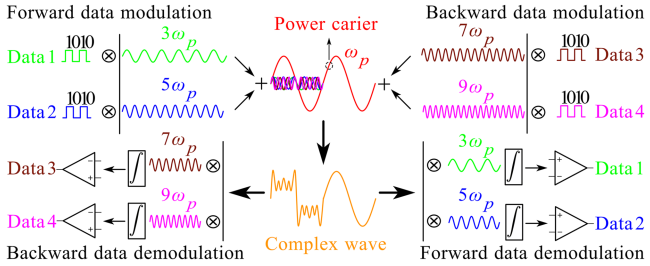

Fig. 7. Modulation and demodulation principle of simultaneous power and four data transmission.

the two sinusoids can be regarded as orthogonal in the interval $[a, b]$, where ω_1, ω_2 are the angular frequencies of the two sinusoids. From the (21), it can be seen that in the sinusoidal function cluster, $\sin(t)$, $\sin(2t)$, $\sin(3t)$, …, $\sin(nt)$ are orthogonal to each other in the interval $[(2k+2)\pi, 2k\pi]$, where n and k are positive integers [20], [21], [22]. Therefore, when some of the function clusters are arbitrarily selected as data carriers, there is no interference between data carriers with different frequencies, even if they are very close in frequency.

The modulation and demodulation principle of simultaneous power and four data transmission is shown in Fig. 7, which contains a power carrier and four data carriers, and the corresponding angular frequencies are ω_p, $3\omega_p$, $5\omega_p$, $7\omega_p$ and $9\omega_p$, respectively. The data modulation is based on the amplitude shift keying (ASK) principle, while the data demodulation is based on the OFDM principle. On the data transmitting side, the forward data 1 and 2 and the backward data 3 and 4 are multiplied by their corresponding data carriers and mixed with the power carrier to transmit. On the data receiving side, the received complex wave is multiplied by the corresponding demodulating waves for integration and threshold comparison to restore the data.

Taking the data 1 transmission process as an example, the power carrier U_p and the data 1 carrier U_{s1} can be expressed as

$$\begin{cases} U_p = U_{mp}\sin(\omega_p t) \\ U_{s1} = U_{ms1}\sin(3\omega_p t + \varphi_1) \end{cases} \tag{22}$$

where U_{mp} and U_{ms1} are the amplitudes of the power and data 1 carriers at the transmitting side, respectively, and φ_1 is the initial phase difference between the data 1 and the power carrier. Based on the 2ASK principle, when the data 1 is "1" or "0," and the corresponding complex wave U_{bit1} and U_{bit0} at the data 1 receiving side can be obtained as

$$\begin{cases} U_{\text{bit1}} = U'_p + U'_{s1} = U'_{mp}\sin(\omega_p t + \Delta\varphi_p) \\ \qquad\qquad +U'_{ms1}\sin(3\omega_p t + \varphi_1 + \Delta\varphi_1) \\ U_{\text{bit0}} = U'_p = U'_{mp}\sin(\omega_p t + \Delta\varphi_p) \end{cases} \tag{23}$$

where U'_p and U'_{s1} are the power and data 1 carriers obtained at the data receiving side, respectively, the U'_{mp} and U'_{ms1} are their amplitudes, and $\Delta\varphi_p$ and $\Delta\varphi_1$ are the phase differences generated by the transmission network.

By multiplying the U'_{s1} with the complex wave U_{bit1} and U_{bit0}, respectively, the functions to be integrated, V_{bit1} and

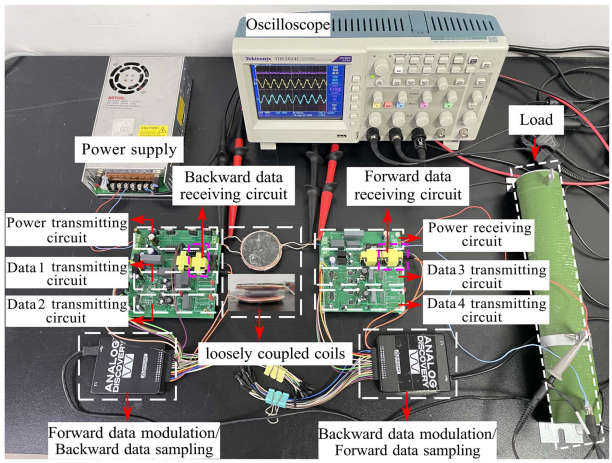

Fig. 8. Experimental platform.

V_{bit0}, can be obtained as

$$\begin{cases} V_{\text{bit1}} = U'_{s1} \times U_{\text{bit1}} \\ \quad = U'_{mp}U'_{ms1}\sin(\omega_p t + \Delta\varphi_p)\sin(3\omega_p t + \varphi_1 + \Delta\varphi_1) \\ \quad\quad + U'^2_{ms1}\sin^2(3\omega_p t + \varphi_1 + \Delta\varphi_1) \\ V_{\text{bit0}} = U'_{s1} \times U_{\text{bit0}} \\ \quad = U'_{mp}U'_{ms1}\sin(\omega_p t + \Delta\varphi_p)\sin(3\omega_p t + \varphi_1 + \Delta\varphi_1) \end{cases} \tag{24}$$

and their integral results can be obtained as

$$\begin{cases} \int_0^T V_{\text{bit1}}dt = \frac{U'^2_{ms1}T}{2} \\ \int_0^T V_{\text{bit0}}dt = 0 \end{cases} \tag{25}$$

where the T is the time period of the power carrier, this is because according to the OFDM principle, the integration period is usually determined by the lowest carrier frequency, and the power carrier is the lowest frequency carrier in the proposed system. It can be seen that the integral results of transmitting data "1" and "0" have a significant difference, so the data can be restored by an appropriate threshold comparison.

V. Experimental Verification

To verify the theoretical analysis of the proposed simultaneous power and multi-channel data transmission method based on OFDM, a 40 W experimental platform is built as shown in Fig. 8. The prototype mainly consists of the power transmitting and receiving circuits, the modulation and sampling modules, the transmitting circuits of data 1–4, the data receiving circuits, the power supply and the load. The outer and inner diameters of the loosely coupled coils are 5.5 and 2 cm, respectively, and the gap is 1 cm, which is probably applicable to portable electronics, smart home appliances, and mobile devices. The specific parameters utilized in the prototype are given in Table I.

The waveforms of power transmission alone are shown in Fig. 9, U_P and U_S are the primary and secondary voltages of the loosely coupled coils, respectively, and U_O is the output voltage on the load R_L. It can be seen that both U_P and U_S are sinusoidal thanks to the good frequency selection characteristics

TABLE I
System Parameters

Parameter	Value	Parameter	Value
R_L	11.5 Ω	C_1	177 nF
L_P, L_S	29 μH	C_2	63.7 nF
M	14 μH	C_3	32.5 nF
L_{f1}, L_{f2}	15 μH	C_4	19.7 nF
C_{f1}, C_{f2}	233 nF	f_p	85 kHz
C_{r1}, C_{r2}	86 nF	f_{s1}	255 kHz
L_1, L_2, L_3, L_4	2.2 μH	f_{s2}	425 kHz
L_{dt}	20 μH	f_{s3}	595 kHz
L_{dr}	20 μH	f_{s4}	765 kHz
U_{dc}	24 V	D_1-D_4	SS26
Q_1-Q_4	IRF540N	-	-

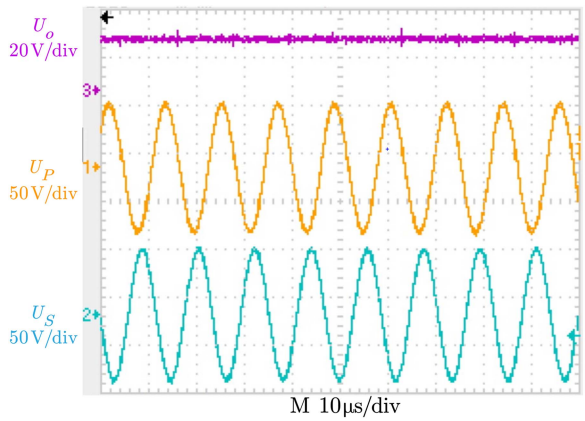

Fig. 9. Waveforms of power transmission alone.

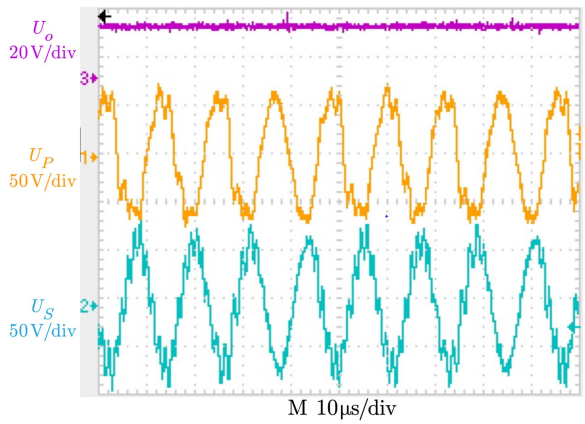

Fig. 10. Waveforms of simultaneous power and four data transmission.

of bilateral *LCC* structure, and the output voltage U_O maintains a stable dc output with a value about 21.3 V. The waveforms of simultaneous power and four data transmission are shown in Fig. 10, and it can be seen that the U_P and U_S have been slightly distorted due to the data transmission, but the output voltage U_O still maintains a good dc output with a value about 21.4 V, which is almost the same as when power is transmitted alone. Therefore, it can be assumed that the power transmission is virtually unaffected by the data transmission.

To verify the constant current output characteristic of the proposed system, the power transmission efficiency η and output

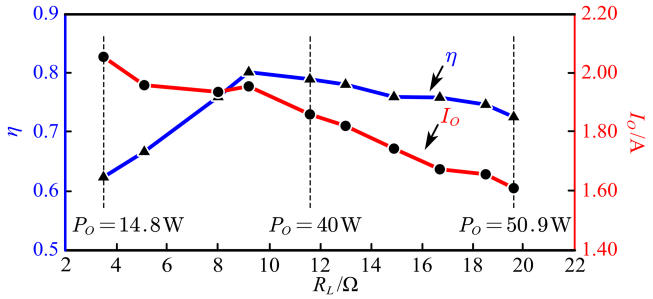

Fig. 11. Efficiency η and output current I_O versus the R_L.

current I_O under different load resistance R_L are shown in Fig. 11. When the R_L increases from 3.5 to 19.6 Ω, the output power P_O increases from 14.8 to 50.9 W, and the R_L is 11.5 Ω for a rated power of 40 W. In the area near the rated power, the efficiency η is about 0.8. Taking the current at the rated power point as a reference, the output current changes from -13% to 10.4%, which is significantly smaller than load resistance variation (±70%), demonstrating that the proposed system has a good current stabilized output characteristic.

To transmit different cyclic data sequences "0101," "1110," "1000," and "0011" into the corresponding four data transfer channels, respectively, and the waveforms of the demodulation process of forward and backward data are shown in Fig. 12.

In Fig. 12, U_{r1} and U_{r2} are the voltages sampled at the forward and backward data receiving sides. In demodulation process based on the OFDM principle, U_{r1} and U_{r2} are integrated after multiplying them with the corresponding data demodulation waves U'_{s1}–U'_{s4}. When the system is initialized, each data carrier is transmitted to the corresponding data receiving circuit individually in sequence, and the corresponding waveforms received by the data receiving circuit are recorded by the software program and used as demodulation waves U'_{s1}-U'_{s4}. The integration period is one power carrier period, and the 85 kbps transmission rate can be obtained for each data. Influenced by the parameter error of experimental components and sampling accuracy, the obtained integration results will have small fluctuations even if the same data are transmitted. However, it can be seen that the integral values of data transmission "0" and "1" have obvious differences, and the corresponding demodulation results can be obtained by selecting the appropriate comparison threshold in every data channel. The threshold is selected to be half of the difference between the average value of the integrals of several data "1" and the average value of several data "0." It is worth noting that the integration results when the transmission data is "0" are not exactly equal to zero, which is due to system parameter errors and switching processes.

The comparison between some typical SWPDT references is given in Table II. Compared with other references, the proposed SWPDT system based on OFDM can achieve two-channel forward and two-channel backward data transmission simultaneously with higher bandwidth utilization. In particular, compared with [15] and [16], which have relatively high power and data transmission rates, the proposed method requires fewer passive components in the data transmission channel and has a simpler

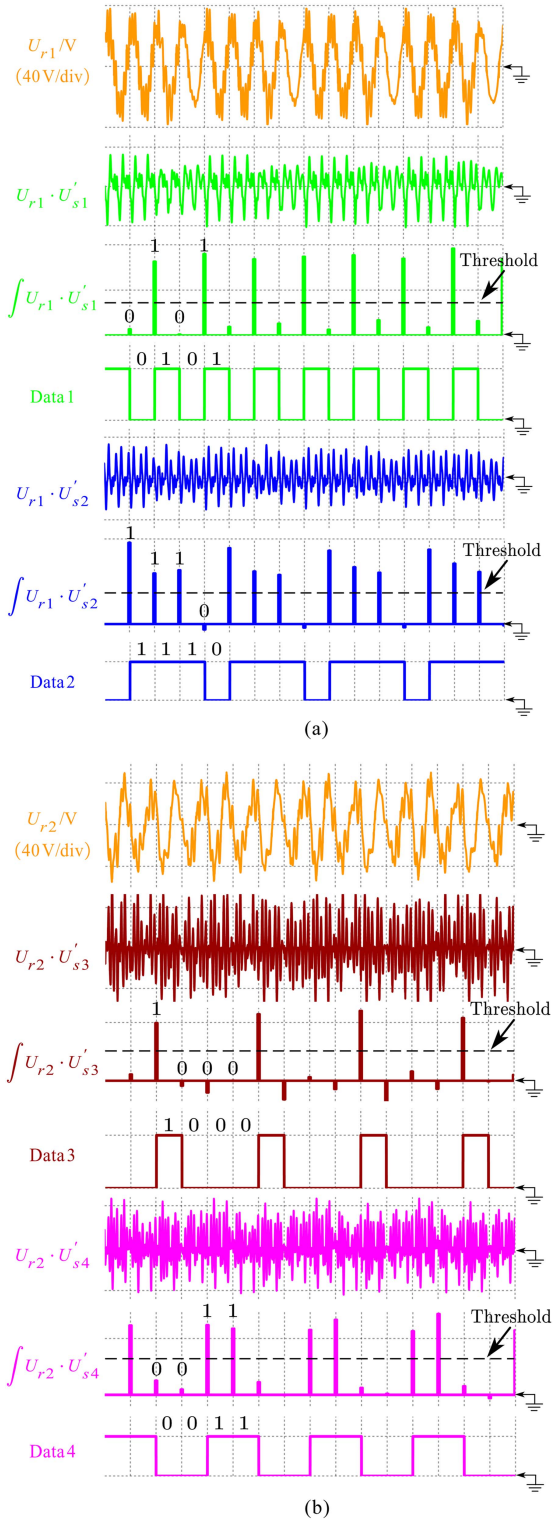

Fig. 12. (a) Demodulation process of forward data. (b) Backward data.

circuit structure. The main advantage of this article over the high power transmission literature [17] is the higher data rate and much lower ratio of carrier frequency to transmission rate. Compared with the literature on multi-channel data communication [18], the proposed method enables full-duplex multi-channel communication with higher data rate.

TABLE II
PERFORMANCE COMPARISON

	This paper	Fan et al. [15]	Wang et al. [16]	Qian et al. [17]	Xia et al. [18]
P_o / W	40	600	400	3300	<35
Modulation	ASK+OFDM	ASK	ASK	DQPSK	PWM
Coils size / cm	5 × 5	-	40 × 40	-	-
Transfer distance / cm	1	-	30	-	-
Data rate / kbps (Forward / Backward)	2 × 85 / 2 × 85	80 / 80	100 / 200	64 / 64	2 × 16 /-
Number of data channel	4	2	2	2	2
Ratio of the carrier frequency to the transmission rate (Forward / Backward)	3, 5 / 7, 9	25 / 15	14 / 21	78 / 97	6.25, 7.5 / -
Average number of passive components per channel	3	10	12	8	3

VI. CONCLUSION

In this article, a simultaneous wireless power and multi-channel data transmission method based on OFDM is proposed. The power transmission uses a bilateral *LCC* compensation structure to suppress the high harmonics generated by the inverter and to achieve load-independent current output. The data transmitting circuits adopt the dual-*LC* resonant networks to achieve two independent data transmitting using only one data transmitting transformer. The modulation of the data adopts 2ASK principle, and the data can be demodulated according to OFDM principle. Moreover, the data receiving circuits do not require any filter circuit and sampling resistor, and the system structure is simplified. The equivalent transfer circuits of the power and data are established, and the system parameters impact on transmission gain is analyzed. Finally, a 40 W experimental platform is built and a 4 × 85 kbps data transmission rate is achieved. Experimental results show that four-channel data in two forward and two backward channels can be transmitted accurately without the interference from power and other data carriers according to the OFDM principle. Moreover, the proposed system exhibits a high data bandwidth utilization.

REFERENCES

[1] Z. Zhang, H. Pang, A. Georgiadis, and C. Cecati, "Wireless power transfer-an overview," *IEEE Trans. Ind. Electron.*, vol. 66, no. 2, pp. 1044–1058, Feb. 2019.

[2] Y. Yao, S. Gao, Y. Wang, X. Liu, X. Zhang, and D. Xu, "Design and optimization of an electric vehicle wireless charging system using interleaved boost converter and flat solenoid coupler," *IEEE Trans. Power Electron.*, vol. 36, no. 4, pp. 3894–3908, Apr. 2021.

[3] Z. Zhang and B. Zhang, "Omnidirectional and efficient wireless power transfer system for logistic robots," *IEEE Access*, vol. 8, pp. 13683–13693, 2020.

[4] S. Roy, A. N. M. W. Azad, S. Baidya, M. K. Alam, and F. Khan, "Powering solutions for biomedical sensors and implants inside the human body: A comprehensive review on energy harvesting units, energy storage, and wireless power transfer techniques," *IEEE Trans. Power Electron.*, vol. 37, no. 10, pp. 12237–12263, Oct. 2022.

[5] X. Li, C. Tang, X. Dai, P. Deng, and Y. Su, "An inductive and capacitive combined parallel transmission of power and data for wireless power transfer systems," *IEEE Trans. Power Electron.*, vol. 33, no. 6, pp. 4980–4991, Jun. 2018.

[6] H. Chen, Z. Cheng, Z. Qian, J. Wu, and X. He, "Application of SWPDT in the feedback control of wireless EV charging," in *Proc. IEEE Energy Convers. Congr. Expo.*, 2020, pp. 1012–1015.

[7] Y. Sun, P.-X. Yan, Z.-H. Wang, and Y.-Y. Luan,, "The parallel transmission of power and data with the shared channel for an inductive power transfer system," *IEEE Trans. Power Electron.*, vol. 31, no. 8, pp. 5495–5502, Aug. 2016.

[8] Y. Jing, W. Feng, K. Qiao, L. Yang, S. Wang, and L. Lu, "Simultaneous wireless power and data transfer system with full-duplex mode based on LCC/CLC resonant network," *IEEE Trans. Power Electron.*, vol. 38, no. 4, pp. 5549–5560, Apr. 2023.

[9] Y. Yao, H. Cheng, Y. Wang, J. Mai, K. Lu, and D. Xu, "An FDM-based simultaneous wireless power and data transfer system functioning with high-rate full-duplex communication," *IEEE Trans. Ind. Inform.*, vol. 16, no. 10, pp. 6370–6381, Oct. 2020.

[10] L. Ji, L. Wang, C. Liao, and S. Li, "Simultaneous wireless power and bidirectional information transmission with a single-coil, dual-resonant structure," *IEEE Trans. Ind. Electron.*, vol. 66, no. 5, pp. 4013–4022, May 2019.

[11] E. S. Lee, "Frequency-modulation-based IPT with magnetic communication for EV wireless charging," *IEEE Trans. Ind. Electron.*, vol. 70, no. 2, pp. 1398–1408, Feb. 2023.

[12] J.-J. Kao, C.-L. Lin, Y.-C. Liu, C.-C. Huang, and H.-S. Jian, "Adaptive bidirectional inductive power and data transmission system," *IEEE Trans. Power Electron.*, vol. 36, no. 7, pp. 7550–7563, Jul. 2021.

[13] J. Kim, G. Wei, M. Kim, H. Ryo, and C. Zhu, "A wireless power and information simultaneous technology based on 2FSK modulation using the dual bands of series-parallel combined resonant circuit," *IEEE Trans. Power Electron.*, vol. vol. 34, no. 3, pp. 2956–2965, Mar. 2019.

[14] H. Li, S. Chen, J. Fang, and K. Wang, "Frequency-modulated phase shift keying communication for MEPT control of wireless power transfer," *IEEE Trans. Power Electron.*, vol. 36, no. 5, pp. 4954–4959, May 2021.

[15] Y. Fan, Y. Sun, X. Dai, Z. Zuo, and A. You, "Simultaneous wireless power transfer and full-duplex communication with a single coupling interface," *IEEE Trans. Power Electron.*, vol. 36, no. 6, pp. 6313–6322, Jun. 2021.

[16] P. Wang, Y. Sun, T. Feng, Y. Fan, and Y. Feng, "Simultaneous wireless power and data transfer system with full-duplex mode based on double-side LCCL and dual-notch filter," *IEEE Trans. Emerg. Sel. Topics Power Electron.*, vol. 10, no. 3, pp. 3140–3151, Jun. 2022.

[17] Z. Qian, R. Yan, J. Wu, and X. He, "Full-duplex high-speed simultaneous communication technology for wireless EV charging," *IEEE Trans. Power Electron.*, vol. 34, no. 10, pp. 9369–9373, Oct. 2019.

[18] C. Xia et al., "Simultaneous wireless power and multibit signals transfer system with hybrid modulation waves PWM control," *IEEE Trans. Power Electron.*, vol. 37, no. 10, pp. 12913–12928, Oct. 2022.

[19] V.-T. Nguyen, V.-B. Vu, G. Gohil, and B. Fahimi, "Coil-to-coil efficiency optimization of double-sided LCC topology for electric vehicle inductive chargers," *IEEE Trans. Ind. Electron.*, vol. 69, no. 11, pp. 11242–11252, Nov. 2022.

[20] H. Yu, S. Guo, Y. Yang, L. Ji, and Y. Yang, "Secrecy energy efficiency optimization for downlink two-user OFDMA networks with SWIPT," *IEEE Syst. J.*, vol. 13, no. 1, pp. 324–335, Mar. 2019.

[21] S. Niu, P. Wang, S. Chi, Z. Liu, W. Pang, and L. Guo, "Enhanced optical OFDM/OQAM for visible light communication systems," *IEEE Wireless Commun. Lett.*, vol. 10, no. 3, pp. 614–618, Mar. 2021.

[22] S. Claessens, Y. T. Chang, D. Schreurs, and S. Pollin, "Receiving ASK-OFDM in low power SWIPT nodes without local oscillators," in *Proc. IEEE Wireless Power Transfer Conf.*, 2019, pp. 20–25.

Yongzhi Jing (Member, IEEE) received the M.S. and Ph.D. degrees in electrical engineering from Southwest Jiaotong University, Chengdu, China, in 2005 and 2014, respectively.

He is currently an Associate Research Fellow with the Department of Electrical Engineering, Southwest Jiaotong University. His main research interests include wireless power transfer, power electronics technology, maglev train and maglev technology.

Xinjie Dan received the B.S. degree in electrical engineering from Xihua University, Chengdu, China, in 2019. He is currently working toward the M.S. degree in power electronics with the Department of Electrical Engineering, Southwest Jiaotong University, Chengdu, China.

His main research interests include wireless power transfer and power electronics technology.

Jialong Yu received the B.S. degree in electrical engineering and automation in 2023 from Southwest Jiaotong University, Chengdu, China, where he is currently working toward the M.S. degree in power electronics with the Department of Electrical Engineering.

His current research interests include wireless energy transfer and sensorless levitation technology.

Kang Fu received the B.S. degree in electrical engineering from Hunan University of Technology, Zhuzhou, China, in 2021. He is currently working toward the M.S. degree in power electronics with the Department of Electrical Engineering, Southwest Jiaotong University, Chengdu, China.

His current research interests include wireless power transfer and power electronics technology.

Suleiman M. Sharkh (Senior Member, IEEE) received the B.Eng. and Ph.D. degrees in electrical engineering from the University of Southampton, Southampton, U.K., in 1990 and 1994, respectively.

He is currently a Professor of Electrical Machines and Drives with the University of Southampton. His main research interests include control, electrical machine, and power electronics with applications to electric vehicles, energy storage, marine propulsion, exhaust energy recovery, submersible pumps and actuators for active vibration control.

Dr. Sharkh was a recipient of the 2008 Engineer Energy Innovation Award for his work on rim-driven thrusters and marine turbine generators. He was also the recipient of The Royal Academy of Engineering ExxonMobil Excellence in Teaching Award in 2013. He is a Member of the Institution of Engineering and Technology and a Chartered Engineer.